




Article

Optical and Morphological Characterization of Nanoscale Oxides Grown in Low-Energy H⁺-Implanted c-Silicon

Anna Szekeres ^{1,*}, Sashka Alexandrova ², Mihai Anastasescu ³, Hermine Stroescu ^{3,*}, Mariuca Gartner ³ and Peter Petrik ^{4,5}

¹ Institute of Solid State Physics, 72, Tsarigradsko Chaussee, 1784 Sofia, Bulgaria

² Department of Applied Physics, Technical University of Sofia, 8 St. Kliment Ohridski Blvd., 1756 Sofia, Bulgaria; salex@tu-sofia.bg

³ Institute of Physical Chemistry “Ilie Murgulescu”, Romanian Academy, 202 Splaiul Independentei, 060021 Bucharest, Romania; manastasescu@icf.ro (M.A.); mgartner@icf.ro (M.G.)

⁴ Institute of Technical Physics and Materials Science, Centre for Energy Research, Hungarian Research Network, Konkoly-Thege Rd. 29-33, 1121 Budapest, Hungary; petrik.peter@ek.hun-ren.hu

⁵ Department of Electrical and Electronic Engineering, Institute of Physics, Faculty of Science and Technology, University of Debrecen, Bem Tér 1, 4032 Debrecen, Hungary

* Correspondence: szekeres@issp.bas.bg (A.S.); hstroescu@icf.ro (H.S.)

Abstract: Nanoscale oxides grown in c-silicon, implanted with low-energy (2 keV) H⁺ ions and fluences ranging from 10¹³ cm^{−2} to 10¹⁵ cm^{−2} by RF plasma immersion implantation (PII), have been investigated. The oxidation of the implanted Si layers proceeded in dry O₂ at temperatures of 700 °C, 750 °C and 800 °C. The optical characterization of the formed Si/SiO_x structures was conducted by electroreflectance (ER) and spectroscopic ellipsometric (SE) measurements. From the ER and SE spectra analysis, the characteristic energy bands of direct electron transitions in Si are elaborated. The stress in dependence on hydrogenation conditions is considered and related to the energy shifts of the Si interband transitions around 3.4 eV. Silicon oxides, grown on PII Si at a low H⁺ fluence, have a non-stoichiometric nature, as revealed by IR-SE spectra analysis, while with an increasing H⁺ fluence in the PII Si substrates and/or the subsequent oxidation temperature the stoichiometric Si-O₄ units in the oxides become predominant. The development of surface morphology is studied by atomic force microscopy (AFM) imaging. Oxidation of the H⁺-implanted Si surface region flattens out the surface pits created on the Si surface by H⁺ implants. Based on the evaluation of the texture index and mean fractal dimension, the isotropic and self-similar character of the studied surfaces is emphasized.

Keywords: low-energy H⁺ ion implantation of c-Si; dry oxidation of H⁺-implanted silicon; UV-vis-IR spectroscopic ellipsometry; electroreflectance spectroscopy; AFM imaging



Citation: Szekeres, A.; Alexandrova, S.; Anastasescu, M.; Stroescu, H.; Gartner, M.; Petrik, P. Optical and Morphological Characterization of Nanoscale Oxides Grown in Low-Energy H⁺-Implanted c-Silicon. *Micro* **2024**, *4*, 426–441. <https://doi.org/10.3390/micro4030027>

Academic Editor: Ajit Roy

Received: 29 April 2024

Revised: 10 July 2024

Accepted: 16 July 2024

Published: 18 July 2024



Copyright: © 2024 by the authors. Licensee MDPI, Basel, Switzerland. This article is an open access article distributed under the terms and conditions of the Creative Commons Attribution (CC BY) license (<https://creativecommons.org/licenses/by/4.0/>).

1. Introduction

Since the invention of integrated circuits in the 1970s, Si technology has followed the mainstream of microelectronic device development toward ever-decreasing element size to the nanometer regime and performance improvements. An important issue is the production of integrated two-dimensional (2D) materials on Si platforms relying on the well-established Si technology for application in computational and non-computational systems. Currently, the major challenge is the control of structures and technological processes in the nanometer range.

In modern devices built on multi-composite and multi-layered structures, often unwanted failure mechanisms occur, mainly triggered by the coefficient of thermal expansion and structural mismatch in the material interfaces, causing reliability problems. Failure mechanisms in electronics have since long been discussed and reviewed in [1,2], where special attention is focused on overstress mechanisms with different physical origins. In silicon-based devices, the stress has been studied intensively in the last decades, discussing

the relation between stress and strain. Everything, however, started with examination of the stress level in the basic Si/SiO₂ interface over which many devices can be integrated for achieving the desired device functionality. Extensive early research results can be found in [3,4].

The stress in Si has been found to be tensile after oxide layers are grown with high compressive levels [5–7]. Lowering the process temperature for reliability and thermal budget issues leads to even higher stress values. A way to control the stress level can be achieved by building a relatively simple layered structure growing SiO₂ on a modified Si surface. This can be realized by applying a dip of the Si surface into a plasma environment, such as plasma ion immersion (PII) implantation [8,9]. The PII implantation method has many advantages over conventional ion implantation and finds an increasing field of applications for surface modification and in the semiconductor industry [9]. Applying this method, the Si subsurface can be modified, creating a depth profile which resembles that calculated by the software program of Stopping and Range of Ions in Matter (SRIM 2010). A suitable environment for such a purpose can be hydrogen plasma through PII of low-energy H⁺ ions. The main advantage of this approach is the ability to change the Si subsurface in a very shallow layer in a controlled way.

The introduction of hydrogen ions into the Si subsurface by PII can have multiple consequences on the subsequent oxidation process. It can allow lowering the oxidation temperature and, at the same time, better control of oxide depth and Si/SiO₂ interface quality. A reasonably lower oxidation temperature can be used because the presence of hydrogen can promote the oxidation process as in wet oxidation, where higher oxidation rates are achieved by the presence of hydroxyl (OH) groups [10–12]. The contribution of H⁺ ions to the oxidation process is twofold: (i) the energetic H⁺ ions from the plasma environment saturate the dangling Si bonds, forming Si-H bonds, and (ii) the H⁺ ions act as catalysts through the formation of H₃O⁺ and OH[−] ion pairs serving as oxidizing agents [4,10,11].

In the present paper, we investigate the formation of nanoscale silicon oxide through incorporation of hydrogen ions (H⁺), introduced into the Si surface layer by plasma immersion implantation (PII) with a low energy of 2 keV. Our attention is focused on the role of hydrogen in the oxide growth process at considerably lowered temperatures as well as in the structural strains generated by the technological processes and in the evaluation of the morphology of the sample surface. Our previous studies [13] have revealed that H⁺ implantation occurs in Si through a ~3 nm thick native SiO₂ layer. The implantation process itself slightly changes the optical properties of the Si surface region, the thickness of which varies between 23 and 13 nm with the H⁺ fluence. The overall effect of shallow implantation of H⁺ is expressed by a low degree of amorphization (up to 5.8%) and generation of weak internal tensile stress arising from implantation-induced defects of vacancies and interstitials [14]. By increasing the H⁺ fluence, the thickness of the modified Si sublayer can be tuned through the formation of highly hydrogenated regions stopping the further penetration of the implanted ions as was established by SE modeling of the modified Si surface layers [13].

The changes in the structure and properties of the few nm thick oxide layers formed in H⁺-implanted Si are studied with highly sensitive optical methods of spectroscopic ellipsometry (SE) and electroreflectance (ER) spectroscopy. Combined with AFM imaging of the development of surface topology of the layers, we can receive useful information on the formation of nanoscale oxides. The conducted studies showed that plasma immersion implantation of H⁺ ions with certain technological parameters results in accelerated oxidation of the H⁺-implanted Si subsurface region yielding more stoichiometric oxides with lower intrinsic oxide stress. AFM imaging revealed a considerably smooth and homogeneous Si surface morphology, which together with the less stressed silicon oxides is an indication for the high-quality oxide surface required in Si technology. The obtained results would help in possible control of the stress level, induced by the technological processes, which has an effect on overall characteristics of the Si-based devices for microelectronics (gate dielectrics,

interlayer dielectric material, capacitor), optoelectronics (energy storage and conversion, sensors), etc.

2. Materials and Methods

2.1. Sample Preparation

In these studies, Cz-grown Wacker single-crystal p-type Si (100) with 4–10 Ω cm resistivity was used as the substrate material. Prior to the implantation process, the substrates underwent a typical Radio Corporation of America (RCA) cleaning procedure [15]. All chemicals used in the RCA cleaning are Merck's "Suprapur" products with 99.99% purity.

Shallow implantation of hydrogen ions was performed in a planar plasma reactor (300 W, 1 kHz) without external heating of the substrates which were biased to 2 kV with pulse repetition frequency of 10 Hz. The energy of the H^+ ions was 2 keV, and the H^+ fluence varied from 10^{13} , 10^{14} to 10^{15} ion/cm², which provided a shallow Si surface layer (a few tens of nm) to be implanted with hydrogen [13].

In order to grow nanoscale oxides into the H^+ -implanted Si surface layer, the implanted substrates together with some non-implanted ones were thermally oxidized in the same runs in dry oxygen (H_2O content < 3 ppm) at atmospheric pressure. The oxides grown into non-implanted Si substrates further served as reference ones. Before oxidation, a fast dip of all samples in diluted (2%) HF was applied to remove any possible surface contaminations. The loading and pulling out proceeded in a dry nitrogen ambience. The oxidation was carried out at temperatures of 700 °C, 750 °C, and 800 °C. The oxidation duration chosen was 30 min at lower temperatures and 20 min at 800 °C, aiming for the oxide layers to be of nearly similar thicknesses. We emphasize that no further thermal treatment was applied to the studied samples.

2.2. Measurement Methods

2.2.1. Spectroscopic Ellipsometry

To record the fine changes caused by the low-energy H^+ implantation in a significantly narrow Si surface layer and to detect the post-oxidation states of the Si/SiO₂ structure, the samples were investigated by spectroscopic ellipsometry (SE) in a wide spectral range covering the UV–visible (UV–vis), near-infrared (NIR) and infrared (IR) regions. For this purpose, the ellipsometric measurements were carried out using two ellipsometers of J. A. Woollam Co., Inc. (Lincoln, NE, USA): one operating in the UV–vis–NIR wavelength, λ , range of 193–1690 nm and the other in the IR spectral range of 300–4000 cm^{−1}. The ellipsometric angles of Ψ and Δ , measured at incident angles of 65° and 70°, were analyzed applying different optical models to the formed Si-SiO_x structures. In the fitting program, an iterative least squares method was used for minimizing the difference (mean square error) between the experimental and theoretical data.

The thickness of the optical layers and their optical constants (refractive index, n , and extinction coefficient, k) were determined from the UV–vis SE spectra with an accuracy of ± 0.2 nm and ± 0.005 , respectively. Further, the dielectric function, ϵ , ($\epsilon = \epsilon_1 - i\epsilon_2$) was calculated. As the absorption in Si strongly increases towards the UV, the optical response comes mainly from a surface layer a few tens of nm thick, which allows studying the behavior of the characteristic peaks of Si at ~ 3.4 eV and ~ 4.2 eV in the ϵ_2 spectra [16]. They are related to interband electrons' direct transitions, and a displacement of peak position relative to that of a stress-free layer can be connected to internal stress generated by the given technology.

The fine change caused in the chemical bonds was traced by the IRSE measurements. The ellipsometric parameters Ψ and Δ were recorded at an angle of incidence of 70° with a resolution of 8 cm^{−1}. IRSE has an excellent sensitivity to absorption of molecules on sample surfaces and to carrier gradients at interfaces. Moreover, from a single IRSE spectrum one can register both the transversal (TO) and longitudinal (LO) vibration modes of atoms in a given chemical bond, receiving additional information about the chemical and structural composition of the layers.

2.2.2. Electroreflectance Spectroscopy

By applying the electroreflectance (ER) spectroscopic method in the 3–4 eV spectral region, we could more closely observe the influence of H^+ implantation on the behavior of the direct bandgap of Si at ~ 3.4 eV. The ER spectra were measured at room temperature using an electrolytic cell with a 0.1 N KCl solution and applying a low external field regime with modulating voltage less than 1 V. Indium contacts were made as Si backside contacts. By using the Aspnes three-point technique [17], the direct transition energy, E_1 , and phenomenological broadening parameter, Γ , were calculated from the analysis of the line shape of ER spectra.

2.2.3. Atomic Force Microscopy

Atomic force microscopy (AFM) measurements were performed in non-contact mode as recommended for minimal tip–sample interaction, with XE-100 AFM from Park Systems (Park Systems Corporate, Suwon, Republic of Korea). All scans were made with NCHR sharp tips from Nanosensors™ (Neuchatel, Switzerland), having less than 8 nm tip radius, ~ 125 μm length, ~ 30 μm width and ~ 42 N/m spring constant/ ~ 330 kHz resonance frequency. The AFM images were recorded at the scale of (1×1) μm^2 . Gwyddion 2.65 (2024 version) was used for 3D image display and Scanning Probe Image Processor software (SPIPTM v. 4.6.0.0) for evaluation of the surface amplitude and spatial parameters.

3. Results and Discussion

3.1. UV-Vis SE Data Analysis

In this section, we present the results of the analysis of the UV–vis SE spectra, investigating the refractive index, density and intrinsic stress of the formed oxides with respect to the process conditions. The thicknesses of the formed oxides are summarized in Figure 1, where the thickness of the oxides grown in non-implanted Si are also presented and referred to hereafter as reference oxides.

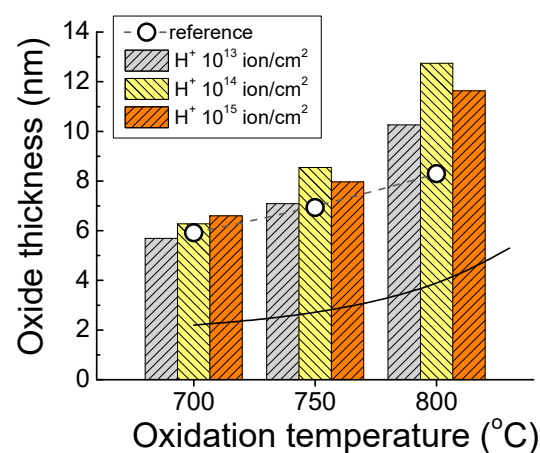


Figure 1. Thickness of the oxides grown in Si, implanted with different H^+ fluences, at 700 °C, 750 °C and 800 °C in dry O_2 . Data for the corresponding reference oxides are shown with empty circles. For comparison, the oxidation kinetics curve (solid line) of standard dry SiO_2 is included.

The oxides on implanted Si are thicker compared to the respective reference ones, indicating the faster oxidation process into the H^+ -modified surface layers [13]. The higher the implantation fluence, the smaller the thickness of the implanted layer is, due to the formation of highly hydrogenated Si subsurface regions that hinder further H-penetration into the Si bulk. The oxidation rates of the reference oxides, grown in non-implanted Si, is also higher as compared to those reported in the literature for dry oxidation of c-Si wafers [18]. This suggests that in the same oxidation run, due to the elevated temperatures, part of the implanted H releases from the samples and could form water molecules or O-H radicals interacting with the neighboring Si surface of reference samples. Most likely, the

presence of hydrogen in the Si subsurface layer or on the Si surface is the cause of faster oxidation, resembling the kinetics of wet oxidation [10]. Obviously, the oxidation kinetics of these samples lies between the standard wet [10] and dry oxidation kinetics of silicon [18] (Figure 1).

Independently of the pre-history of the oxidized samples, the refractive index values decreased with increased oxidation temperature. This is illustrated in Figure 2 for the oxides grown into H^+ -implanted Si substrates at 700 °C, 750 °C and 800 °C. As can be seen, the reference oxides have considerably higher refractive index values, pointing to the rather high compressive stress generated during the dry oxidation process due to lattice mismatch between SiO_2 and Si substrate and, consequently, to volume expansion occurring in the oxidation process [14]. However, H^+ implantation creates favorable conditions for the growth of oxides in a less dense and tense Si structure [13]. Most probably, the presence of hydrogen provides a larger amount of Si dangling bonds formed during the implantation process in an amorphized Si subsurface layer, which facilitates the faster growth of oxides at considerably lowered temperatures.

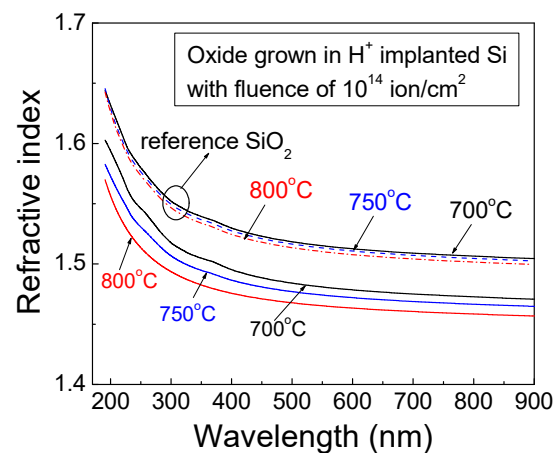


Figure 2. Dispersion spectra of the refractive index of oxides grown at 700 °C, 750 °C and 800 °C in Si (100), implanted with H^+ 10^{14} ion/cm² fluence. Spectra for reference oxides grown in non-implanted Si (100) at corresponding temperatures are included.

Using the above ellipsometric data of the refractive index values, the oxidation-induced stress in grown oxides can be estimated. Assuming that the observed changes in the oxide density and its refractive index are caused by elastic compression, the oxide stress can be calculated from the first-order compressibility, expressed as $n_{ox} = n_0 + (\Delta n / \Delta \sigma) \sigma$ [19], where σ is the stress and $\Delta n / \Delta \sigma$ is the compressive coefficient and taken for silica equal to 9×10^{-12} m²/N. The refractive index n_0 is equal to 1.46 for a free-of-stress SiO_2 . Historically, the mechanical stress values are usually calculated at a single wavelength (usually at $\lambda = 633$ nm), as these values give the tendency of evaluation of built-in stress during the processes. Therefore, we estimated the oxidation-induced stress from the n_{ox} values also at $\lambda = 633$ nm to be comparable with the reported values by other authors for other technological conditions and thicker oxides. The stress values estimated from the refractive indices represent the total oxide stress, which is the sum of the thermally-induced stress due to differences in the thermal expansion of the Si and SiO_2 and the intrinsic oxide stress generated by its growth. Here, we examine the total stress without extracting the thermal stress component, since the intrinsic oxide stress we estimated later when considering the dielectric functions. The results are summarized in Figure 3. The stress in the oxides grown in non-implanted Si is compressive and shows a tendency to slightly decrease with an increase in the oxidation temperature from 700 °C to 800 °C, temperatures which in principle are considered to be low in Si technology. The oxide stress for the H^+ -implanted samples shows a tendency to increase with increasing H^+ fluence for a given temperature and to decrease with enhanced temperature, but its level remains considerably lower in

all cases compared to that for reference oxides. Apparently, the presence of H species in a PII-modified, less dense Si subsurface layer promotes/facilitates the release of process-induced structural strains in the oxide matrix. As a result, at 800 °C the oxidation-induced stress level becomes an order of magnitude lower regardless of the H⁺ fluence during PII (Figure 3).

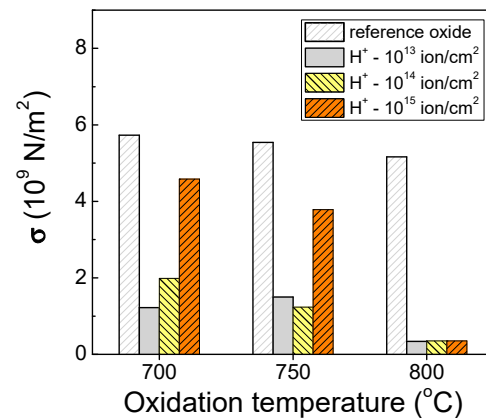


Figure 3. Total oxide stress versus oxidation temperature estimated from the refractive index values taken at $\lambda = 633$ nm for reference oxide and oxides grown on H⁺-implanted Si.

The refractive index is a measure of oxide density, and the relationship can be described by the Lorentz–Lorenz equation of $\rho = K(n^2 - 1)/(n^2 + 2)$, where $K = 8.046$ for thermal SiO₂ [20]. The calculated oxide density, ρ , values are given in Table 1 together with the corresponding refractive indices, n , and intrinsic oxide stress, σ . It is worth mentioning that a fully relaxed amorphous SiO₂ has a density of 2.2 g/cm³ [21] and a refractive index equal to $n = 1.46$, as was mentioned above. According to the observations [19–21], by reducing the oxidation temperature the oxide density increases, as is the case for our reference oxides. However, the oxides grown on H⁺-implanted Si do not follow this trend; on the contrary, with increases in the temperature, the oxide density decreases. This is most likely due to an intense release of hydrogen with increases in temperature, forming voids and thus reducing the density of the material, helping to release the oxidation-induced stress, which results in an overall effect of smaller refractive indices, lower intrinsic stress and density of the oxide layers, as seen in Table 1.

Table 1. Variation of oxide parameters (n , ρ , σ) with H⁺ fluence and oxidation temperature, T_{ox} .

H ⁺ Fluence (ion/cm ²)	T_{ox} (°C)	Refractive Index, n at $\lambda = 633$ nm	Oxide Density, ρ (g/cm ³)	Oxide Stress, σ (10 ⁹ N/m ²)
-	700	1.511	2.411	5.67
10 ¹³	700	1.471	2.250	1.22
10 ¹⁴	700	1.477	2.275	1.89
10 ¹⁵	700	1.501	2.366	4.56
-	750	1.510	2.406	5.56
10 ¹³	750	1.473	2.257	1.44
10 ¹⁴	750	1.471	2.250	1.22
10 ¹⁵	750	1.493	2.240	3.67
-	800	1.467	2.232	0.78
10 ¹³	800	1.457	2.192	0.33
10 ¹⁴	800	1.459	2.199	0.11
10 ¹⁵	800	1.462	2.214	0.22
Standard dry oxidation *	700	1.475	2.265	1.67
	750	1.473	2.257	1.44
	800	1.472	2.253	1.33
	1000	1.465	2.224	0.56

* The oxidation parameters are for standard dry oxidation of Si wafers at different temperatures, taken from Ref. [20].

In addition, we analyzed the dielectric function ϵ , and in particular the imaginary part of ϵ represented the light absorption in the studied structures. Since the oxide layers are several nanometers thick, the two characteristic peaks of the underlying Si (E_1 appearing at 3.4 eV and E_2 at 4.2 eV) [22] can be observed in the ϵ_2 spectra of the pseudodielectric functions $\langle\epsilon\rangle$ of the Si in the presence of a nanoscaled oxide top layer. Any deviation of the position of these peaks from those of unstrained silicon gives additional information about the internal strains generated by the technological processes [5,23]. Because the uncertainties in the experimental and iterative errors increase toward the UV region, we will examine only the behavior of the E_1 peaks in the $\langle\epsilon_2\rangle$ spectra. The displacements of the E_1 peak position are in a meV range and thus, for more precise determination of the peak position, we differentiated the $\langle\epsilon_2\rangle$ dependence on photon energy E , as the peak position is obtained at $d\epsilon_2/dE = 0$. The results are summarized in Figure 4.

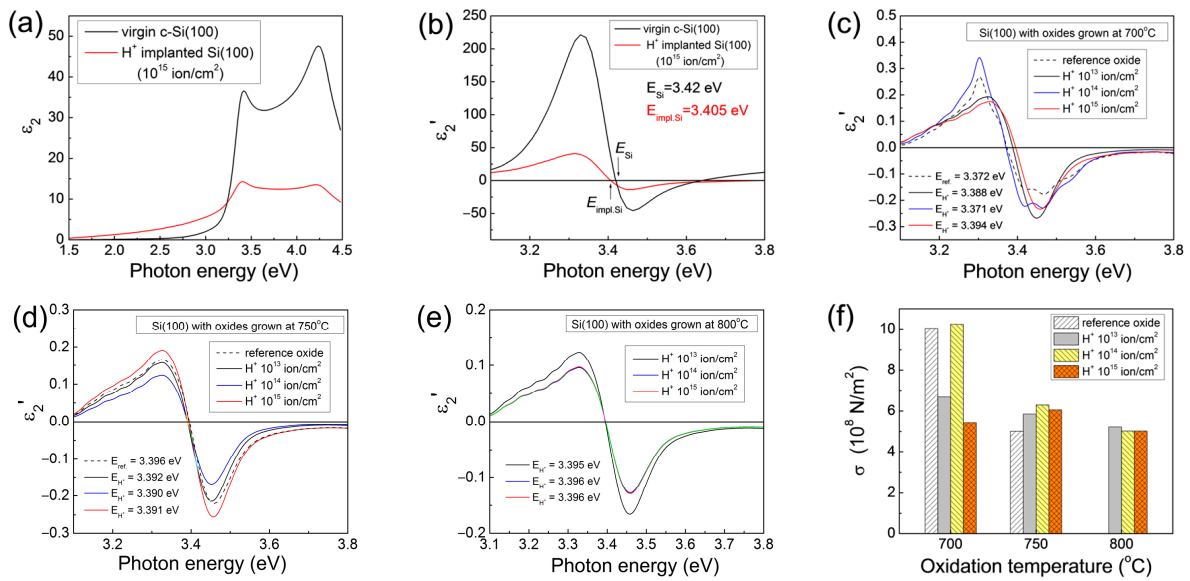


Figure 4. Imaginary part ϵ_2 of the dielectric function, ϵ , of a virgin c-Si (100) and after its implantation with H^+ ion fluence of 10^{15} ion/cm² (a) and their first derivative (b). The corresponding first derivative of $\langle\epsilon_2\rangle$ for Si (100) implanted with different H^+ fluences and oxidized at 700 °C (c), 750 °C (d) and 800 °C (e) up to nanoscale thicknesses given in Figure 1; evaluated stress at the Si–SiO₂ interface, formed by oxidation of the H^+ PII silicon at different technological conditions (f).

The position of the E_1 peak of the virgin non-implanted Si (100) substrate is at $E_1 = 3.42$ eV and is shifted toward $E_1 = 3.405$ eV by increasing the fluence of implanted H^+ ions up to 10^{15} ion/cm² (see Figure 4b). The magnitude of the E_1 displacement varies with the given technological processes, and its values are included in the corresponding figures in Figure 4. For oxides grown at higher temperatures on hydrogen-implanted Si, the displacement of E_1 is smaller. Knowing the E_1 peak positions, the corresponding stress levels can be calculated from the relationship of $\Delta E_1 \times c$, where c is the correlation coefficient and equal to 2.09×10^{10} Nm^{−2}eV^{−1} for thermally grown SiO₂ [5]. The results are presented in Figure 4f. As is seen, structural stress values, generated in the oxide and appearing at the Si–SiO₂ interface, are in the order of 10^8 N/m² and well correlated to those reported in the literature [5,18,19]. However, at a low (700 °C) temperature, the oxidation of H^+ -implanted silicon generates smaller structural strains at the Si–SiO₂ interface in comparison to those of the reference oxides, which is most likely due to a beneficial effect of the presence of hydrogen species in the layer-growing process. By increasing the oxidation temperature, an overall reduction in the stress can be observed.

3.2. Electreflectance Spectroscopy

The investigated non-implanted and oxidized Si reference samples exhibit ER spectra with the shape and polarity typical for the p-type Si substrate. For the H⁺-implanted Si samples, gradual change is observed, and for a 10¹⁵ ion/cm² H⁺ fluence, the polarity of the ER spectra is inverted. In Figure 5, as an example, the ER spectra for oxides grown at 700 °C and 750 °C on implanted Si with a H⁺ fluence of 10¹⁵ cm⁻² are given. The opposite ER signal for the highest ion fluence is indicative of an inversion of the surface field [24] and can be attributed to the thin subsurface layer with implantation defects. The defect concentration, however, cannot be high, since otherwise it would hinder the ER signal [17].

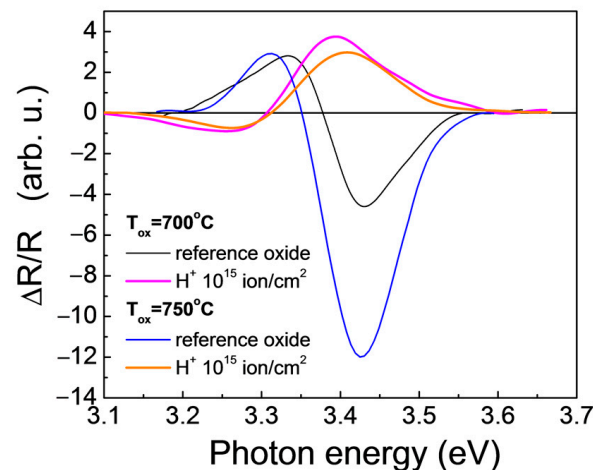


Figure 5. ER spectra for oxides grown in dry O₂ at 700 °C and 750 °C in non-implanted and implanted Si (100) with H⁺ fluence of 10¹⁵ ion/cm².

ER spectra allow critical point energies and broadening parameters to be obtained directly and precisely from experimental data without requiring data reduction by Kramers–Kronig analysis [17]. From the ER spectra analysis, the direct transition, which occurs between the valence and the conduction band at the center of the Brillouin zone, referred to as a direct Si energy gap, E_1 , and its broadening parameter, Γ , were determined. The results are presented in Table 2. In the electron band structure of silicon, the transition at room temperature appears as a single transition at $E_g = 3.4$ eV. The transition energies at around this value for all samples are shifted relative to that of the unstressed silicon surface, which is in our case $E_1 = 3.42$ eV of the non-implanted c-Si (100) (Figure 4b). Therefore, the shifts are indicative for internal stress developed in the Si during oxidation. The evaluated tensile stress levels and the broadening parameter Γ in Si as a function of the H⁺ fluence are also presented in Table 2. In the calculation of the stress from energy transition shifts, the correlation coefficient of $2.09 \times 10^{10} \text{ Nm}^{-2}\text{eV}^{-1}$ was used [5]. The values indicate a low level of tensile stress at the Si surface, which corresponds to compressive stress in the oxide resulting from post-implantation oxidation.

The increase in the parameter Γ as compared with non-implanted Si samples seems reasonable because the generated defects in the Si subsurface layer by the plasma ionization during implantation cannot be annealed at the post-implantation oxidation temperatures. In any case, the Γ values, being around 100 meV, can be considered to be small [25]. This, together with the relatively small Si stress levels, points to improved oxide quality as a result of the presence of H atoms in the Si space-charge region during implantation.

Table 2. Si parameters of transition energy, E_1 , broadening parameter, Γ , and Si stress level, σ , at different H^+ fluences and oxidation temperatures, T_{ox} .

H^+ Fluence (ion/cm ²)	T_{ox} (°C)	Polarity of Lineshape	Transition Energy, E_1 (eV)	Si Stress Level, σ (10 ⁸ N/m ²)	Broadening Parameter, Γ (meV)
-	700	"+"	3.397	6.44	95
10 ¹³	700	"+"	3.398	6.16	110
10 ¹⁴	700	"+"	3.406	3.92	120
10 ¹⁵	700	"−"	3.390	8.40	110
-	750	"+"	3.399	5.88	95
10 ¹³	750	"+"	3.408	3.36	100
10 ¹⁴	750	"+"	3.409	3.08	115
10 ¹⁵	750	"−"	3.392	7.84	125

3.3. IRSE Data Analysis

Usually, the Fourier-transform infrared (FTIR) spectra published in the literature are taken with unpolarized light, and thus, only the TO modes can be detected. However, using polarized light, our IRSE measurements could register both TO and LO modes as well. The ellipsometric angles Ψ and Δ were recorded at an angle of incidence of 70° with a resolution of 8 cm^{−1}. At the IRSE data analysis, a two-layer optical model and Bruggeman's effective medium approximation theory were applied, as the oxide layer was considered as a mixture of Si, SiO₂ and SiO, while the surface roughness layer was considered as a mixture of 50% material (oxide) and 50% voids (air). The IRSE spectral analysis was conducted on the oxidized Si implanted with H^+ ions.

Although the ellipsometric data Ψ and Δ are interrelated and the exact position of the vibration modes of the existing chemical bonds cannot be directly determined, conclusions can be drawn from the specific features, registered in the measured spectra. An example is given in Figure 6, where the regions with specific features, connected with chemical bonds of Si-O, Si-H and O-H, are marked in Figure 6a.

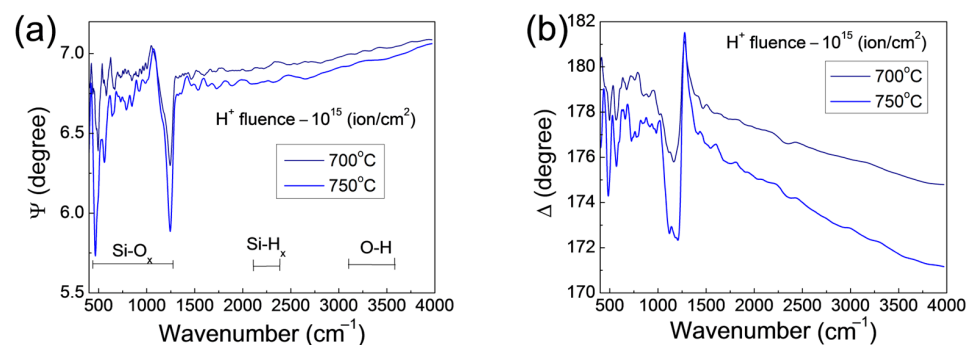


Figure 6. IRSE spectra of ellipsometric angles Ψ (a) and Δ (b) of H^+ -implanted Si (fluence 10¹⁵ ion/cm²) after its thermal oxidation at 700 °C and 750 °C in dry O₂.

As can be seen, in the spectral region below 1500 cm^{−1}, multiple intense features are registered. On the contrary, in the spectral range of 1500–4000 cm^{−1}, relatively smooth variation with very weak features is observed. Vibration modes, attributed to H-related bonds in different configurations, if any, might be detected as H-Si(O₃) at ~875 cm^{−1} [26], SiH_x ($x = 1, 2, 3$) in the 2200–2300 cm^{−1} range [27–29], O-H hydroxyl groups (3300–3600 cm^{−1}) [30] and molecular H₂O at ~1640 cm^{−1} [28]. In our case, in these regions no or very weak features can be seen, which disappear at the ellipsometric data modeling. The absence of clear H bonding can be explained by the release of H and/or OH from the as-grown layer during the oxidation process, H playing rather a catalytic role in the oxidation process. The ob-

served accelerated growth of reference oxides in dry O_2 (Figure 1) supports this assumption. The possible residual hydrogen concentration must be rather low to be detected.

The peaks related to rocking oscillations of oxygen atoms in Si-O bonds appear in the range of $440\text{--}460\text{ cm}^{-1}$ (TO) and $503\text{--}510\text{ cm}^{-1}$ (LO) [31]. The bands at 805 cm^{-1} and $\sim 814\text{ cm}^{-1}$ are related to TO and LO bending oscillations of Si atoms in Si-O units, respectively [31]. The stretching oscillation of bridging O atoms in the Si-O units is manifested in the bands in the range of $1010\text{--}1150\text{ cm}^{-1}$ (TO) and $1180\text{--}1300\text{ cm}^{-1}$ (LO) [31]. Due to the nanoscale thickness of our oxides, the characteristic Si-O bands are expected to appear at lower frequencies in comparison to thick (over $\sim 200\text{ nm}$) stoichiometric SiO_2 layers [32]. Moreover, it has been reported that deviation from the stoichiometric composition also could cause a shift toward lower frequencies of the position of Si-O vibration modes [29].

According to the above observations, further only the $400\text{--}2000\text{ cm}^{-1}$ IRSE region is considered where the vibrational bands related to Si-O chemical bonds are well pronounced. This is well seen in Figure 7, where the dispersion dependencies of n and k are presented for oxides grown into non-implanted and H^+ -implanted Si at 700°C . The IR spectra of the samples oxidized at 750°C and 800°C are not given here because they have similar shapes and trends. The obtained dispersion curves are well correlated to those reported for thin silicon oxide grown at temperatures below 1000°C [33,34].

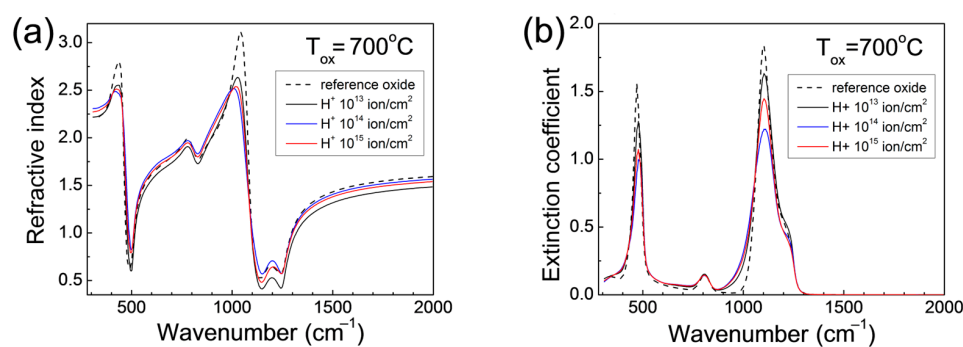


Figure 7. Dispersion curves of the refractive index (a) and extinction coefficient (b) in the spectral range of $300\text{--}2000\text{ cm}^{-1}$ for silicon oxide layers formed at oxidation temperature of 700°C in Si substrates implanted with different H^+ ion fluences.

Further, we analyzed the optical characteristics which contain information about the absorption properties, namely, the imaginary ε_2 part of the dielectric function ε and the dielectric loss function $\text{Im}(-1/\varepsilon)$. In Figure 8, as an example, the results for the Si samples implanted with a H^+ ion fluence of 10^{14} ion/cm^2 and subsequently oxidized at different temperatures are given.

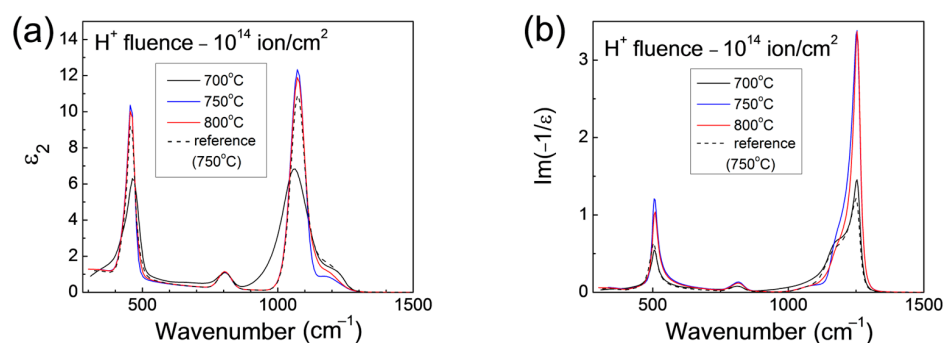


Figure 8. IRSE spectra of the imaginary part ε_2 of the dielectric function ε (a) and the dielectric loss function $\text{Im}(-1/\varepsilon)$ (b) of silicon oxide layers grown at different temperatures in Si, implanted with H^+ fluence of 10^{14} ion/cm^2 . Data for reference oxide grown in non-implanted Si at 750°C are shown.

The complex shape of the spectral bands in Figure 8 implies the existence of Si-O chemical bonding in different configurations. To obtain better insights, we deconvoluted the main Si-O bands into Gaussian components. The obtained multiple Gaussian peaks with close positions to each other suggest that the Si-O chemical bonds could be with different bond angles or configurations [35,36]. For illustration purposes, in Figure 9 the deconvoluted main peaks with the Gaussian components, related to the stretching vibrational mode of oxygen, are shown for oxides grown at different temperatures in Si implanted with a H^+ fluence of 10^{13} ion/cm².

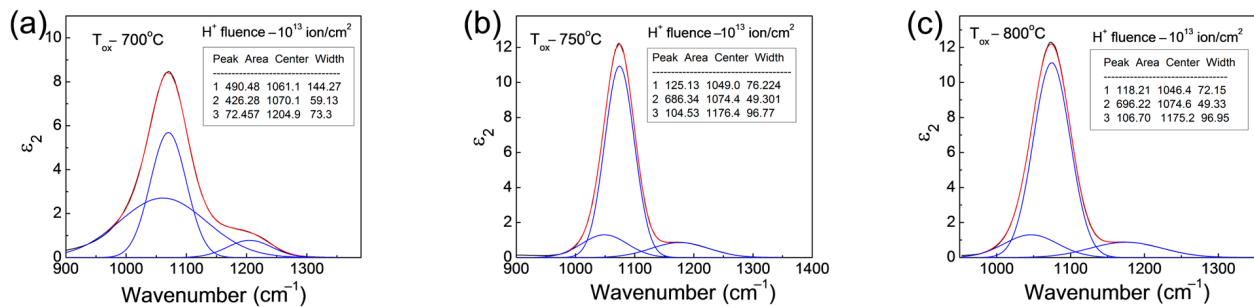


Figure 9. Deconvolution in Gaussian components of the main peak related to stretching vibrational mode of oxygen in oxides grown at temperatures of 700 °C (a) 750 °C (b) and 800 °C (c) in Si implanted with H^+ fluence of 10^{13} ion/cm².

We have deconvoluted into Gaussians all vibrational modes related to Si-O bonds, and the results are summarized in Table 3. The frequency shift of the TO and LO modes as a function of the implanted hydrogen fluence and of the oxidation temperature is well demonstrated. These bands are related to vibration of oxygen atoms bonded to Si in different configurations, suggesting that the grown oxides contain also non-stoichiometric SiO_x ($1 < x < 4$) units.

Table 3. Peak positions in ϵ_2 and $Im(-1/\epsilon)$ spectra as a function of H^+ ion fluence and oxidation temperature, T_{ox} .

H^+ Fluence (ion/cm ²)	T_{ox} (°C)	Peak Position (cm ⁻¹)											
		In the ϵ_2 Spectrum						In the $Im(-1/\epsilon)$ Spectrum					
0	700	444	460	805	1073	1074	1169	504	813	1157	1182	1240	1254
	750	422	458	805	1073	1093	1202	503	814	1156	1178	1237	1253
	800	-	460	805	1075	1077	1205	508	815	-	1180	1245	1254
10^{13}	700	408	462	805	1061	1070	1205	508	813	1129	1195	1246	1255
	750	440	460	805	1045	1074	1176	508	816	1172	1178	1232	1252
	800	438	460	805	1046	1075	1175	507	815	1168	1192	1245	1255
10^{14}	700	446	471	805	1062	1063	1216	506	813	1114	1192	1245	1255
	750	440	460	805	1048	1074	1177	508	816	1166	1190	1243	1254
	800	427	458	805	1073	1077	1179	509	817	1171	1188	1243	1255
10^{15}	700	455	465	805	1056	1069	1210	506	813	1128	1182	1236	1253
	750	442	459	805	1048	1074	1178	508	816	1163	1184	1238	1253

The peak position of oxygen vibration in non-stoichiometric $Si-O_2-Si_2$ complexes appears around ~ 1045 cm⁻¹ (TO) and ~ 1190 cm⁻¹ (LO), while in $Si-O_3-Si$ units it appears around 1070 cm⁻¹ (TO) and $Si-O-Si_3$ at ~ 1130 cm⁻¹ (LO) [35,36]. Usually, for stoichiometric $Si-O_4$ tetrahedral units, the peaks are around ~ 1090 cm⁻¹ (TO) and ~ 1250 cm⁻¹ (LO) [37]. As has been reported, at nanoscale oxide thicknesses the peak positions move toward lower frequencies [32,38]. Therefore, it can be expected that the observed peaks at ~ 1074 cm⁻¹ (TO) and 1238 – 1246 cm⁻¹ (LO), respectively, can be attributed to the vibration band of oxygen in stoichiometric $Si-O_4$ units.

In dependence on the technological conditions, the amount of Si-O₃-Si, Si-O₄ and Si-O₂-Si₂ complexes changes. In Figure 10, these changes are demonstrated by the variation of the main characteristic peak area in the IR spectra. Each area of the Gaussian peaks is normalized to the total peak area. At low temperature and low H⁺ fluence, the predominant complex in the oxides is the non-stoichiometric Si-O₃-Si bonds. By increasing the temperature, the oxide becomes more stoichiometric and the Si-O₄ configuration predominates (Figure 10b,c).

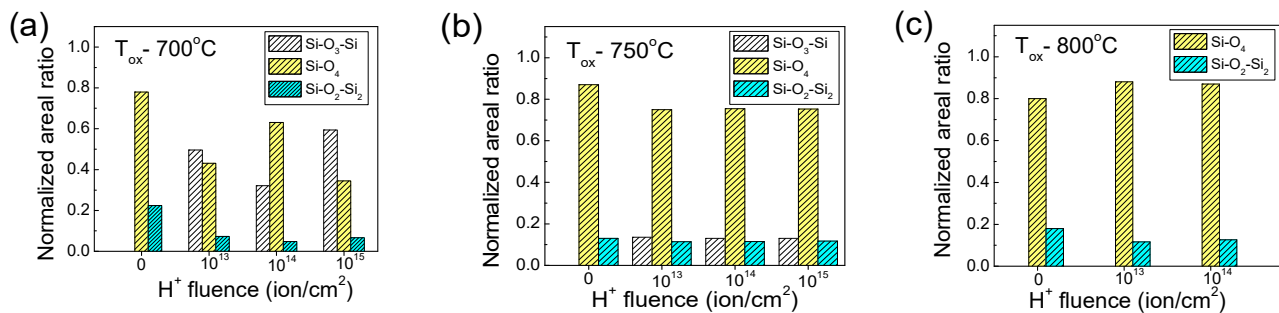


Figure 10. Variation of chemical bonding of Si-O complexes with the H⁺ ion fluence and oxidation temperatures of 700 °C (a), 750 °C (b) and 800 °C (c). The data are related to the main characteristic peak in 1000–1300 cm^{−1} spectral region.

Based on the above results, we can conclude that the optimal temperature for oxidation of H⁺-implanted Si surface layers is 750 °C, which results in a nearly stoichiometric SiO₂ layer (Figure 10b) and an acceptable low level of intrinsic oxide stress (Figures 3 and 4f).

3.4. AFM Imaging

In this section, the morphology of oxide surfaces resulting from the certain technological processes used is examined by AFM imaging. The results are summarized in Figure 11, where the 3D AFM topographic images recorded from 1 μm × 1 μm scanned areas are presented. In the figure, the 3D images display the surface of the nanoscale oxides grown in implanted c-Si (100) with low-energy hydrogen ions at fluences of 10¹³, 10¹⁴ and 10¹⁵ ion/cm² (from left to right) at temperatures of 700 °C, 750 °C and 800 °C (from top to bottom). In our previous studies of the surface quality of samples prepared by similar technological conditions and sequence, as used herein, the amplitude parameters of root mean square roughness (*S_q*), surface skewness (*S_{sk}*) and surface kurtosis (*S_{ku}*) were discussed [39,40]. Since these AFM parameters are very similar to those reported in [39,40], we bring here into discussion the roughness average, *S_a*, (defined as the arithmetic average of the absolute values of the profile height deviations) and the peak-to-peak height, *S_y*, (defined as the height difference between the highest and lowest pixel in the image). The reason is that, in view of practical applications of the studied specimens, the peak-to-valley parameter (*S_y*) is more intuitive and can be understood as the thickness of the roughness layer (comparable with the thickness of the roughness, calculated in Spectroscopic Ellipsometry).

Besides the amplitude parameters, two other spatial parameters [41] were evaluated for the implanted and oxidized samples, namely the texture direction index, *S_{tdi}*, and the mean fractal dimension, MFD. Mathematically, the texture direction index, *S_{tdi}*, is a measure of the dominant direction (defined as the average amplitude sum divided by the amplitude sum of the dominating direction), but here we use it as a measure of the sample's isotropy (if *S_{tdi}* > 0.5, then the surface is isotropic). The MFD (calculated for different angles by analyzing the Fourier amplitude spectrum) gives a hint about the self-similarity of the sample, in other words, the property of the sample to “replicate” its topography in areas.

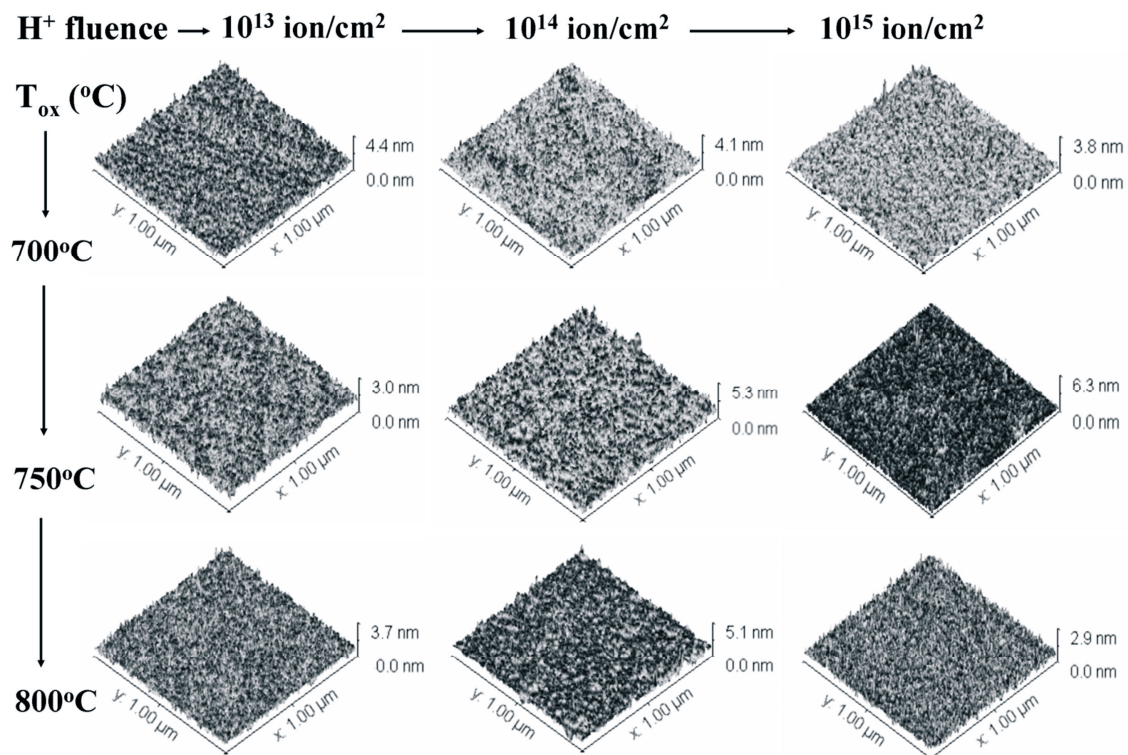


Figure 11. Three-dimensional AFM topographic images recorded at the scale of $1\ \mu\text{m} \times 1\ \mu\text{m}$, ordered by increasing H^+ fluence from left to right and by increasing the oxidation temperature from top to bottom.

The amplitude parameters S_a and S_y together with the spatial parameters S_{tdi} and MFD are plotted in Figure 12. It is worth mentioning that, when comparing the reference (non-implanted Si substrates) [39] with the implanted and oxidized specimens, an increase in roughness can be noticed.

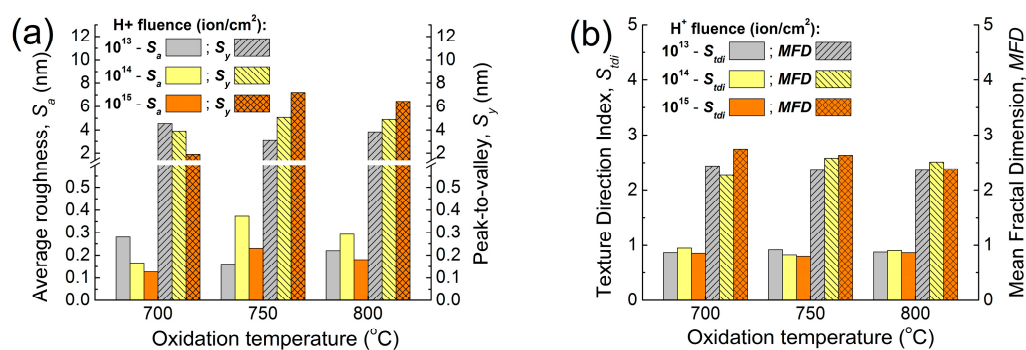


Figure 12. The amplitude (average roughness, S_a and peak-to-valley, S_y) (a) and spatial parameters (texture direction index, S_{tdi} , and mean fractal dimension, MFD) (b) as a function of the oxidation temperature for oxides grown in H^+ -implanted Si with different ion fluences.

In the samples implanted at a $10^{13}\ \text{ion/cm}^2$ H^+ fluence (first column in Figure 11), where the average roughness S_a does not overcome 0.3 nm, it can be observed that the peak-to-valley parameter S_y has a slight decrease for the sample oxidized at 750 °C, then exhibiting a slight back-increase after oxidation at 800 °C. However, even at 800 °C, the S_y parameter does not exceed 4 nm over a $1 \times 1\ \mu\text{m}^2$ scanned area. Both spatial parameters are specific for isotropic surfaces in these samples (H^+ $10^{13}\ \text{ion/cm}^2$), while the mean fractal dimensions MFD values are well below 2.5, being specific for smooth surfaces.

For the samples implanted at a 10^{14} ion/cm² H⁺ fluence (middle column in Figure 11), some randomly distributed local non-homogeneities are present, which are most probably formed during the oxidation process. This is reflected in the increase in the roughness parameters, as the S_y values increase from ~4 nm to ~5 nm by increasing the oxidation temperature from 700 °C to 750 °C, and in the average roughness (S_a), which doubles its value from 0.17 to 0.37 nm. Simultaneously, the texture direction index, S_{tdi} , undergoes a slight decrease caused by the appearance of local non-uniformities (irregular oxide clusters), but the samples preserve the isotropic texture.

For the samples, implanted at a 10^{15} ion/cm² H⁺ fluence (right column in Figure 11), after an abrupt increase in roughness parameters (both S_a and S_y) with the temperature (from 700 °C to 750 °C), there is a tendency toward flattening, as at 800 °C the surface becomes more uniform and less corrugated with increasing S_{tdi} values (isotropic character).

4. Conclusions

In the present paper, the results from a thorough study of the properties of nanoscale oxides, grown on Si (100) implanted with hydrogen at low energy, are discussed. Beneficial effects were found, such as increased oxidation rates at relatively low temperatures in the interval 700 °C–800 °C, decreased Si–SiO₂ interface and oxide stresses and improved surface morphology.

It can be concluded that the implantation with low-energy light H⁺ ions did not seriously damage either the Si surfaces or the Si subsurface layers, as evidenced by the low stress levels estimated by SE and ER spectral analyses and AFM morphology. Hydrogen atoms most probably have a catalytic role, increasing the oxide growth. Their presence in the Si subsurface layers creates conditions for growing nearly stoichiometric oxides with lower refractive indices and less intrinsic stresses at low temperatures, unusual in Si technology.

From the point of view of silicon technology, the conducted studies can recommend the optimal temperatures of 750 °C and 800 °C for oxidation of low-energy H⁺ ion-implanted Si surface layers, which yield a stoichiometric SiO₂ layer and significantly low level of oxide stress.

From the UV–vis, IRSE and AFM topography results, it can also be concluded that hydrogen promotes structural ordering of the oxide and the interface with the Si, which predicts better electrical characteristics of Si–SiO₂ structures being building blocks in Si-based devices.

Our research makes some contributions to the demand for improved performance of integrated circuits and electronic devices for the development of increasingly complex applications in many industrial branches. This has created the need for new manufacturing processes along with new metrological challenges to adequately monitor process control in silicon technology during the fabrication of advanced nanostructures.

Author Contributions: Conceptualization, A.S., S.A. and M.A.; writing—original draft preparation, A.S., S.A, M.A. and H.S.; writing—review and editing, A.S., S.A., M.A., M.G. and P.P.; data curation, H.S., A.S, M.A., S.A. and P.P.; supervision, A.S. and S.A; project administration, A.S. and M.G. All authors have read and agreed to the published version of the manuscript.

Funding: This research received no external funding.

Institutional Review Board Statement: Not applicable.

Informed Consent Statement: Not applicable.

Data Availability Statement: The data presented in this study are available on request from the corresponding authors.

Acknowledgments: The authors gratefully acknowledge the support of this work in the frame of Academic Exchange Programs between the Bulgarian and Hungarian Academies of Sciences and the Romanian Academy. This work was partially supported within the research program “Science of Surfaces and Thin Layers” from the “Ilie Murgulescu” Institute of Physical Chemistry. Support

from the National Research, Development and Innovation Office (NKFIH) in Hungary through the Grant OTKA K-146181 is gratefully acknowledged. TKP2021-EGA04 has been implemented with the support provided by the Ministry of Innovation and Technology of Hungary from the NRD Fund under the funding scheme TKP2021. The authors express their gratitude to Mihai Stoica from ALS Life Sciences, Romania for providing the data of the IRSE spectra.

Conflicts of Interest: The authors declare no conflicts of interest.

References

- Menon, S.; Stecki, C.; Song, J.; Pecht, M. Optimization of PHM System for Electronic Assemblies Using Maintenance Aware Design Environment Software. In Proceedings of the 14th Australian International Aerospace Congress, Melbourne, VIC, Australia, 28 February–3 March 2011.
- Available online: <https://www.Semitracks.Com/Newsletters/May/2021-May-Newsletter.Pdf> (accessed on 22 April 2024).
- Ikeda, S.; Ohta, H.; Miura, H.; Hagiwara, Y. Mechanical Stress Control in a VLSI-Fabrication Process: A Method for Obtaining the Relation between Stress Levels and Stress-Induced Failures. *IEEE Trans. Semicond. Manuf.* **2003**, *16*, 696–703. [\[CrossRef\]](#)
- Leroy, B. Stresses and silicon interstitials during the oxidation of a silicon substrate. *Philos. Mag. B* **1987**, *55*, 159–199. [\[CrossRef\]](#)
- Fitch, J.T.; Bjorkman, C.H.; Lucovsky, G.; Pollak, F.H.; Yin, X. Intrinsic Stress and Stress Gradients at the SiO₂/Si Interface in Structures Prepared by Thermal Oxidation of Si and Subjected to Rapid Thermal Annealing. *J. Vac. Sci. Technol. B Microelectron. Process. Phenom.* **1989**, *7*, 775–781. [\[CrossRef\]](#)
- Lane, C.H. Stress at the Si—SiO₂ interface and its relationship to interface states. *IEEE Trans. Electron Devices* **1968**, *15*, 998–1003. [\[CrossRef\]](#)
- Szekeres, A. Stress in The SiO₂/Si Structures Formed by Thermal Oxidation. In *Fundamental Aspects of Ultrathin Dielectrics on Si-Based Devices*; Springer: Dordrecht, The Netherlands, 1998; pp. 65–78.
- Li, Z.; Chen, F. Ion Beam Modification of Two-Dimensional Materials: Characterization, Properties, and Applications. *Appl. Phys. Rev.* **2017**, *4*, 011103. [\[CrossRef\]](#)
- Gupta, D. Plasma Immersion Ion Implantation (PIII) Process-Physics and Technology. *Int. J. Adv. Technol.* **2011**, *2*, 471–490.
- Tomoizawa, M. Water Diffusion in Silica Glass and Wet Oxidation of Si: An Interpretation for the High Speed of Wet Oxidation. *J. Electrochem. Soc.* **2011**, *158*, G115. [\[CrossRef\]](#)
- Mott, N.F. On the oxidation of silicon. *Philos. Mag. B* **1987**, *55*, 117–129. [\[CrossRef\]](#)
- Mott, N.F.; Rigo, S.; Rochet, F.; Stoneham, A.M. Oxidation of silicon. *Philos. Mag. B* **1989**, *60*, 189–212. [\[CrossRef\]](#)
- Szekeres, A.; Alexandrova, S.; Petrik, P.; Fodor, B.; Bakalova, S. Ellipsometric Study of Crystalline Silicon Hydrogenated by Plasma Immersion Ion Implantation. *Appl. Surf. Sci.* **2013**, *281*, 105–108. [\[CrossRef\]](#)
- Volkert, C.A. Stress and Plastic Flow in Silicon during Amorphization by Ion Bombardment. *J. Appl. Phys.* **1991**, *70*, 3521–3527. [\[CrossRef\]](#)
- Kern, W.; Puotinen, D. Cleaning Solutions Based on Hydrogen Peroxide for Use in Silicon Semiconductor Technology. *RCA Rev.* **1970**, *31*, 187–206.
- Daunois, A.; Aspnes, D.E. Electoreflectance and Ellipsometry of Silicon from 3 to 6 eV. *Phys. Rev. B* **1978**, *18*, 1824–1839. [\[CrossRef\]](#)
- Misiewicz, J.; Sitarek, P.; Sęk, G. Photoreflectance Spectroscopy of Low-Dimensional Semiconductor Structures. *Opto-Electron. Rev.* **2000**, *8*, 1–24.
- Irene, E.A.; Ghez, R. Thermal Oxidation of Silicon: New Experimental Results and Models. *Appl. Surf. Sci.* **1987**, *30*, 1–16. [\[CrossRef\]](#)
- Fargeix, A.; Ghibaudo, G. Densification of Thermal SiO₂ Due to Intrinsic Oxidation Stressing. *J. Phys. D Appl. Phys.* **1984**, *17*, 2331–2336. [\[CrossRef\]](#)
- Irene, E.A.; Tierney, E.; Angilello, J. A Viscous Flow Model to Explain the Appearance of High Density Thermal SiO₂ at Low Oxidation Temperatures. *J. Electrochem. Soc.* **1982**, *129*, 2594–2597. [\[CrossRef\]](#)
- Taniguchi, K.; Tanaka, M.; Hamaguchi, C.; Imai, K. Density Relaxation of Silicon Dioxide on (100) Silicon during Thermal Annealing. *J. Appl. Phys.* **1990**, *67*, 2195–2198. [\[CrossRef\]](#)
- Jellison, G.E. Optical Functions of Silicon Determined by Two-Channel Polarization Modulation Ellipsometry. *Opt. Mater.* **1992**, *1*, 41–47. [\[CrossRef\]](#)
- Nguyen, N.V.; Chandler-Horowitz, D.; Amirtharaj, P.M.; Pellegrino, J.G. Spectroscopic Ellipsometry Determination of the Properties of the Thin Underlying Strained Si Layer and the Roughness at SiO₂/Si Interface. *Appl. Phys. Lett.* **1994**, *64*, 2688–2690. [\[CrossRef\]](#)
- Seraphin, B.O. Electoreflectance in Surface Physics. *J. Phys. Colloq.* **1970**, *31*, C1-123–C1-134. [\[CrossRef\]](#)
- Karachevtseva, L. Quantum-Sized Effects in Oxidized Silicon Structures with Surface II-VI Nanocrystals. *Semicond. Phys. Quantum Electron. Optoelectron.* **2014**, *17*, 168–173. [\[CrossRef\]](#)
- Zamchiy, A.O.; Baranov, E.A.; Merkulova, I.E.; Khmel, S.Y.; Maximovskiy, E.A. Determination of the Oxygen Content in Amorphous SiO_x Thin Films. *J. Non. Cryst. Solids* **2019**, *518*, 43–50. [\[CrossRef\]](#)

27. Marra, D.C.; Edelberg, E.A.; Naone, R.L.; Aydil, E.S. Silicon Hydride Composition of Plasma-Deposited Hydrogenated Amorphous and Nanocrystalline Silicon Films and Surfaces. *J. Vac. Sci. Technol. A Vac. Surf. Film.* **1998**, *16*, 3199–3210. [[CrossRef](#)]
28. Hsieh, Y.L.; Kau, L.H.; Huang, H.J.; Lee, C.C.; Fuh, Y.K.; Li, T.T. In Situ Plasma Monitoring of PECVD Nc-Si:H Films and the Influence of Dilution Ratio on Structural Evolution. *Coatings* **2018**, *8*, 238. [[CrossRef](#)]
29. Carneiro, J.O.; Machado, F.; Rebouta, L.; Vasilevskiy, M.I.; Lanceros-Méndez, S.; Teixeira, V.; Costa, M.F.; Samantilleke, A.P. Compositional, Optical and Electrical Characteristics of SiO_x Thin Films Deposited by Reactive Pulsed DC Magnetron Sputtering. *Coatings* **2019**, *9*, 468. [[CrossRef](#)]
30. Theil, J.A.; Tsu, D.V.; Watkins, M.W.; Kim, S.S.; Lucovsky, G. Local Bonding Environments of Si–OH Groups in SiO₂ Deposited by Remote Plasma-Enhanced Chemical Vapor Deposition and Incorporated by Postdeposition Exposure to Water Vapor. *J. Vac. Sci. Technol. A Vac. Surf. Film.* **1990**, *8*, 1374–1381. [[CrossRef](#)]
31. Lehmann, A.; Schumann, L.; Hübner, K. Optical Phonons in Amorphous Silicon Oxides. I. Calculation of the Density of States and Interpretation of LO-TO Splittings of Amorphous SiO₂. *Phys. Status Solidi* **1983**, *117*, 689–698. [[CrossRef](#)]
32. Martinet, C.; Devine, R.A.B. Comparison of Experimental and Calculated TO and LO Oxygen Vibrational Modes in Thin SiO₂ Films. *J. Non. Cryst. Solids* **1995**, *187*, 96–100. [[CrossRef](#)]
33. Tan, C.Z. Determination of Refractive Index of Silica Glass for Infrared Wavelengths by IR Spectroscopy. *J. Non. Cryst. Solids* **1998**, *223*, 158–163. [[CrossRef](#)]
34. Kitamura, R.; Pilon, L.; Jonasz, M. Optical Constants of Silica Glass from Extreme Ultraviolet to Far Infrared at near Room Temperature. *Appl. Opt.* **2007**, *46*, 8118. [[CrossRef](#)]
35. Revesz, A.G. The Defect Structure of Vitreous SiO₂ Films on Silicon. I. Structure of Vitreous SiO₂ and the Nature of the Si–O Bond. *Phys. Status Solidi* **1980**, *57*, 235–243. [[CrossRef](#)]
36. Lisovskii, I.P.; Litovchenko, V.G.; Lozinskii, V.B.; Frolov, S.I.; Flietner, H.; Fussel, W.; Schmidt, E.G. IR Study of Short-Range and Local Order in SiO₂ and SiO_x Films. *J. Non. Cryst. Solids* **1995**, *187*, 91–95. [[CrossRef](#)]
37. De Los Arcos, T.; Müller, H.; Wang, F.; Damerla, V.R.; Hoppe, C.; Weinberger, C.; Tiemann, M.; Grundmeier, G. Review of Infrared Spectroscopy Techniques for the Determination of Internal Structure in Thin SiO₂ Films. *Vib. Spectrosc.* **2021**, *114*, 103256. [[CrossRef](#)]
38. Lisovsky, I.P.; Lytovchenko, V.G.; Mazunov, D.O.; Szekeres, A. IR-Spectroscopy Analysis of the Structure and Composition of the Si–O Phase in Ultrathin (10–15 nm) SiO₂ Films. *Ukr. J. Phys.* **2005**, *50*, 78–83.
39. Anastasescu, M.; Stoica, M.; Gartner, M.; Bakalova, S.; Szekeres, A.; Alexandrova, S. Surface Morphology of RF Plasma Immersion H⁺ Ion Implanted and Oxidized Si(100) Surface. *J. Phys. Conf. Ser.* **2014**, *514*, 012036. [[CrossRef](#)]
40. Szekeres, A.; Alexandrova, S.; Terziyska, P.; Anastasescu, M.; Stoica, M.; Gartner, M. Study of Silicon Surface Layers Modified by Hydrogen Plasma Immersion Ion Implantation and Oxidation. *J. Phys. Conf. Ser.* **2020**, *1492*, 012056. [[CrossRef](#)]
41. Image Analysis Software for Microscopy. Available online: <https://www.imagemet.com/> (accessed on 25 April 2024).

Disclaimer/Publisher’s Note: The statements, opinions and data contained in all publications are solely those of the individual author(s) and contributor(s) and not of MDPI and/or the editor(s). MDPI and/or the editor(s) disclaim responsibility for any injury to people or property resulting from any ideas, methods, instructions or products referred to in the content.